Hindawi
International Journal of Aerospace Engineering
Volume 2021, Article ID 9497683, 13 pages
https://doi.org/10.1155/2021/9497683

Research Article

Research on the Fatigue of Small Impulse Turbine Blade Based on the Numerical Simulation and Experimental Tests

Shijie Liu[1], **Guozhu Liang**[2], **Jichao Liu**[3], **Yichuan Yang**[4] and **Hui Wang**[1]

[1]*Beijing Aerospace Propulsion Institute & Laboratory of Science and Technology on Cryogenic Liquid Propulsion, Beijing 100076, China*
[2]*School of Astronautics, Beihang University, Beijing 102206, China*
[3]*Beijing Machine Tool Research Institutive-Precision Mechatronics CO., LTD., Beijing 100102, China*
[4]*School of Mathematical Sciences, Beihang University, Beijing 102206, China*

Correspondence should be addressed to Guozhu Liang; lgz@buaa.edu.cn

Received 5 November 2019; Revised 5 December 2020; Accepted 27 January 2021; Published 10 February 2021

Academic Editor: Jeremy Straub

Reusable spacecraft is increasingly attracting researchers' attention. However, the experimental investigations on the turbine blade of the rocket engine are rarely published. Thus, the fatigue of a small impulse rocket turbine blade is explored in the current work. First, the specimen and the electrode of electrical discharge machining are carefully designed. Then, the electrical discharge machining is used to machine the specimen. To study the fatigue properties, the finite element analyses are separately performed on the blade model and the specimen. Based on the numerical results, a fatigue test is carried out to reproduce the most vulnerable position. Finally, the microstructural structures of the specimen are detected using the scanning electron microscope (SEM). Results show that (1) different from the aviation field, the specimen is unable to be machined with the welding method because it destroys the crucial details and the mechanical properties; (2) the maximum plastic strain is present at the leading edge close to the hub, at which a 760 μm corner crack appears at the 10113th fatigue cycle. This work provides a feasible method of using the EDM process to machine specimen for the small impulse turbine blade.

1. Introduction

From the 1970s, the reusable space shuttle has been widely studied by the USA and the Soviet Union. Although the shuttle had to retire from 2011 due to its high launch cost, developing reusable spacecraft is still an increasingly interesting development direction. As well-known, in the liquid rocket engine, the turbine is widely used to pressure the liquid propellants. However, life-related experimental investigations for turbine blades were rarely reported in the aerospace field because the testing specimen is difficult to be prepared and the tests are always expensive. Indeed, many relevant efforts have been taken in the aviation field. For example, the creep-fatigue life of a turbine blade made from full-scale directionally solidified alloy was investigated in [1], where the full-scale hollow turbine blade was fixed by the disk and the special clamp. To conduct the thermomechanical fatigue test on the single crystal turbine blade with the cooling hole, in 2013, Wang et al. [2] developed a special test rig, by which the crack was successfully reproduced by using the heating and cooling subsystem to model the takeoff and shutdown stage in flight, respectively. In 2016, Jing et al. [3] proposed a thermomechanical fatigue (TMF) life assessment method for a single crystal turbine blade, where the aerodynamical bending is realized by adjusting the spacers on the clamp. In 2016, Cao and Yan [1] conducted the creep/fatigue tests on the full-scale turbine blade, in which the temperature gradient was reasonably governed by the screw mounted on a specially designed clamp. In 2020, Sanaye and Hosseini [4] used the thermodynamics, turbo-machinery, and artificial network models to predict the blade working life of an industrial gas turbine at off-design conditions, from which it is seen that the operating parameters mainly affect the convective heat transfer coefficients over the inside and outside surfaces of the blade. Additionally, it also shows that the load ratio and the inlet temperature influence the rotor blade life

cycle exponentially. Besides, there are numerous literature concerning the microstructural variations caused by the service conditions. In 2014, Tawancy and Al-Hadhrami [5] examined the microstructural variations of the first-stage turbine blades protected by the Cr-modified aluminide coating, which are exposed to the same service conditions as that in an electric power plant. Results indicate that the superalloy composition and the operating temperature are the critical factors influencing the microstructure changes. In 2020, Zhang et al. [6] studied the microstructural degradation during the rejuvenation heat treatment of directionally solidified turbine blades, where results suggest the service-exposed blade suffers from coalescence and coarsening of the γ' -phase, transformation of carbides, and precipitation of a topological close-packed phase.

From the above statements, it is seen the tests at the laboratory are widely for life assessment of specimen degree. Thus, how to prepare the specimen is an interesting problem in the experiment. Generally, the blade specimens are mainly processed by two methods, i.e., welding and casting. Two main issues should be carefully taken into account during the specimen preparation. First, how to exert loads on the specimen is to model the working condition of the real blade? Second, how to machine the specimen to keep its mechanical properties are consistent with the real blade. For example, to address the two problems, in 2016, the blade-like specimens were, respectively, manufactured by the welding and max-casting method by Wang et al. [7], and a comparison was made to find the advantages of individual processing methods. From [7], it is seen that the welding method has two drawbacks: (1) the strength of the welded parts are weaker than the tested part, leading to unexpected failure at the welded portion; (2) the tested portion is possible to be destroyed during the welding processing especially when the specimen is very small. In contrast, the two drawbacks are not present in the casting method. However, to the best knowledge of the authors, the casting method is unsuitable to be widely used in the laboratory because of its huge cost. Thus, the investigation on preparing the specimen of an impulse turbine blade with a small size is rarely published.

As an advanced machining method, the EDM process is investigated in the current work to find whether it is suitable to prepare the small blade specimen. About the EDM techniques, a review was conducted in [8], where the surface modification with the EDM process is investigated and some applications are also discussed. Abbas et al. [9] presented some types of EDM techniques and discussed the developing trend of the EDM process. In 2018, Tanjilul et al. pointed out that [10] the surface quality of the EDM process is influenced by many factors. Thus, to get the needed surface quality, some investigations are performed to find the optimal sets of the machining parameters. In 2018, Agarwal et al. [11] investigate how to maximize the Material Removal Rate (MRR) and minimize the surface roughness (Ra) based on the multiple regression and Jaya algorithm, where the pulse current (IP), pulses on time (Ton), duty cycle (Tau), and gap voltage (V) are the independent variables. Additionally, in 2018, Nagaraju et al. [12] applied the Fuzzy method and the Taguchi algorithm to investigate the response of the EDM process. In the optimization, the multiple responses are separately converted to a single characteristic index. On the other hand, in 2018, Dastagiria et al. [13] used the multi-objective optimization to study the optimal EDM process parameters. Different from the single-objective optimization, the MRR, Ra, and Tool Wear Rate (TWR) are separately taken as the objective function. In 2018, Prakash et al. [14] employed the multiobjective particle swarm algorithm to optimize the EDM process parameters optimization to deposit the HA coating. In the optimization, the surface roughness, thickness of the recast layer, and microhardness were chosen as the response characteristics. In 2019, Zhou et al. [15] established a closed-loop control system for the EDM to improve its process performances. By adapting the gap servo-voltage, the process efficiency was remarkably improved. Comparing the integral blade rotors with assembled discs, the component weight is reduced up to 20-30%, increasing the efficiency considerably, reducing at the same time the fuel consumption and gas emissions. In [16], the authors reviewed the manufacturing processes of integral blade rotors for turbomachinery. They pointed out that the selection of machining processes for blade depends on the as-received material. Furthermore, the authors suggest the EDM process causes a molten metal superficial layer (with different properties than base material) that affects fatigue response. Compared with the milling, the wire electrodischarge machining and sink electrodischarge machining, the EDM process has the most economical roughing process for nickel-base material.

From the above analyses, it is found that it is a critical but difficult matter to prepare the blade specimen, and the method of processing small specimens is rarely published. Thus, in the current paper, two methods, the welding and the EDM, are compared to process the specimen for a type of impulse turbine blade. After comparison, the electrical discharge machining (EDM) is selected to machine the specimen. First, the specimen is specially designed in order to satisfy the experimental requirements. Second, the specimen is machined with the EDM. Then, to release the residual stresses and remove the defects in the specimen, the sand-blasting treatment was adopted to improve its surface quality. The microstructures at the corner of the leading edge are analyzed with the SEM. Note the features are determined by the authors' experience because the key problem in the investigation is to find the suitable method of machining the specimen but not to the optimal machining parameters. The feasibility of this processing method is supported by the finite element analysis, the microstructure detection, and the fatigue test.

2. Methodology

The real turbine explored in the current work is manufactured with the integral molding casting method. One part of the turbine is displayed in Figure 1.

From Figure 1, it is seen that the size of the impulse turbine blade is rather small. Because the energy cycle of the rocket engine belongs to the open type, the impulse airfoil is selected to obtain the high-pressure ratio. Moreover, although the cooling holes are not present in the blade, the

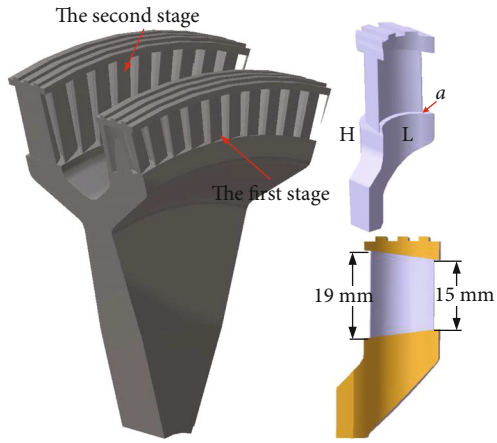

Figure 1: Parts of the turbine rotor.

shape of the airfoil is still complicated. Note that if the inlet total temperature of the turbine is high, the cooling holes will be used to protect the blade, which will influence the aerodynamical performance due to the secondary flow and limit the blade lifespan because of the stress concentration.

2.1. Designing Blade Specimen. The blade and its specimen should hold two major features: (1) the critical parts to be verified are the same; (2) the fundamental mechanical properties are the same, which should not to be destroyed during the machining. Besides, the aerodynamical forces and other causes influencing the blade working life are also needed to be considered in the design phase. Some relevant literatures can be found in [2, 17].

In the current work, the design rules of the specimen are summarized as follows:

(1) The deformation caused by the aerodynamical force is not considered due to the small starting torque and the excellent material's mechanical properties

(2) The blade will be used in the turbine who's inlet total temperature is only dozens of Kelvin, which nearly has no influence on the blade

(3) The pressure generally has little influence on the life of the blade, so the pressure effect is not considered herein

According to these three rules, the clamps and the tested blade of the specimen are designed coaxially. Two clamping parts are used to exert the loads representing the centrifugal force. In fact, the fatigue of the current blade is the interaction of the LCF and HCF, which are separately caused by the start-up/shutdown and the high-frequency vibration. The study of this interaction will be as a future work.

2.2. Selecting Machining Method. Generally, two machining methods are commonly used in the aviation field to prepare the specimen, i.e., the welding and casting method. In the current work, the two machining methods are used to prepare the blade specimen. The specimen (Figure 2) is first processed with the CO_2 shielded arc welding method.

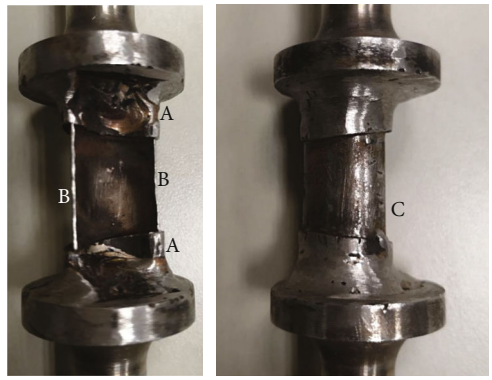

Figure 2: Welded blade specimen.

As shown in Figure 2, it is seen that the specimen has poor processing quality. From the perspective of the geometrical features, the critical portions, "A" and "C," are dramatically destroyed. Additionally, the blade leading and trailing edges "B" are also destroyed by the splash of the molten metal. Importantly, the design requirement of the coaxial between the blade and the clamps are not ensured during the process. From the above analyses, it is obvious the CO_2 shielded arc welding method is unsuitable to manufacture such a small blade specimen.

Additionally, in 2020, Zink et al. [18] investigated the manufacturing processes for the liquid rocket turbopump impeller, and they pointed out that the conventional milling, electronic welding, laser welding, and 3D printing are effective processing methods. In the laser welding processing, a laser is used as the heat source. As the laser heats the metal pieces and melts the metal, the gap between the components acts as a capillary for the solder to flow and bond the components. Laser welding has the advantages of high energy density, low heat input, small structural deformation, no vacuum environment, high quality, high precision, high efficiency, etc., and is the leader in all kinds of fusion welding methods for metal material. Indeed, in 2015, Oguma et al. [19] introduced some manufacturing techniques for high-efficiency gas turbines, in which the laser metal deposition welding method was employed to repair the damaged turbine blade. From the repair process, it is seen the welding method is slightly complicated. Thus, this method is not considered in the current work. Actually, the pulse argon arc welding machine, equipment cost, and running cost are much lower than laser welding machine, which is also widely used in the aircraft and rocket turbine manufacturing and repair [20]. From [21], it is seen that the laser additive 3D printing is used to manufacture the turbine blade. For laser additive printing, a powder of metal alloy is spread in a thin layer by the printing machine. A computer-controlled laser then fuses the powder into a cross-section of the engine component. The machine spreads a second layer of powder, and the process repeats until the component is complete. Although the above-stated processing methods have many advantages, however, they are still not widely employed at the university laboratory because of various reasons, such as the small-batch and the few processing resources.

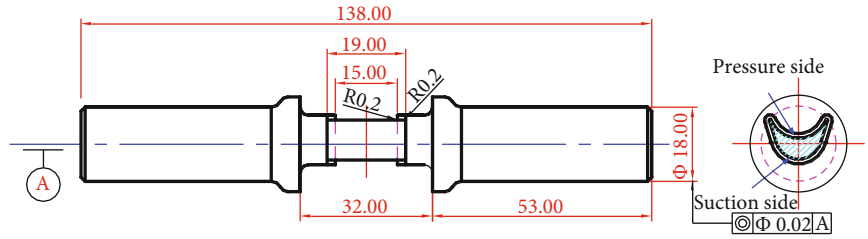

Figure 3: Layout of the designed specimen.

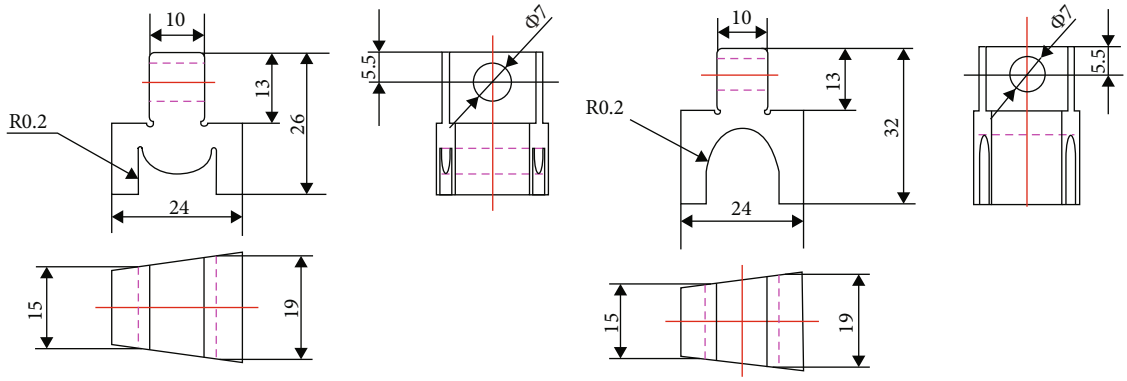

(a) Used for suction side processing

(b) Used for pressure side processing

Figure 4: Layouts of electrode 702.

Table 1: Performances of GW735.

Item	Value
Maximum machining efficiency(copper-steel)	400 mm^3/min
Peak current	64 A
The best surface roughness	*Ra* 0.2
Minimum electrode wear	0.1%
Pulse power type	Isopulse power during discharge

Note that the roughness of Ra0.2 cannot be achieved by using 64 A current. In fact, the data in Table 1 are the limit performance index of GW735, which means the maximum current of the equipment can reach 64 A, and the maximum processing efficiency can reach 400 mm^3/min under certain conditions, and the best surface roughness can reach Ra0.2 under another condition. Instead of using the same electrode, in the current work Ra0.2 is obtained using two sets of different electrodes.

Theoretically, the casting method can be used to machine any complex specimen unless the casting mold is well-prepared. However, the high processing cost limits the application of this method. The application of the casting method can be found in [2], where the principle of the casting method of preparing the specimen are summarized as follows:

(1) The shroud and the fortress (or hub) are far away from the critical section, i.e., the casted shroud has little effect on the critical portions

(2) The casting mold can be readily obtained by designing the specimen based on the existing blade model

Unfortunately, through many attempts, the two methods are not suitable to machine the specimen of this type of impulse turbine blade. Finally, the EDM is selected to machine the specimen because of the following advantages:

(1) It keeps the fundamental geometrical details compared with the welding method

(2) It is easier and cheaper to design and machine the electrode than prepare the casting model

(3) It is suitable to machine such a small specimen with a complicated profile than the traditional machining methods

2.3. Machining Program. The machining program consists of four main parts:

(1) Machining the 304SS round bar on the lathe to obtain the clamps

(2) Using the copper electrode set to machine the transition parts

(3) Using the copper electrode set to machine the tested part, i.e., the testing blade model

(4) Using the sandblasting treatment to release the residual stresses and remove the defects from the specimen

2.4. Feasibility Analysis. To verify the feasibility of the EDM process method, the finite element analysis is separately

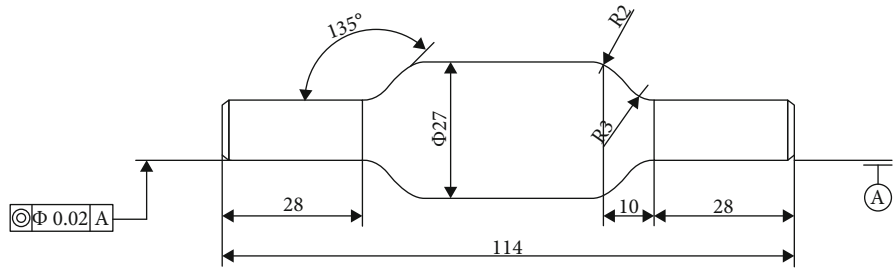

(a) Processing features

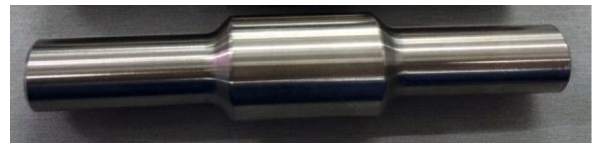

(b) Appearance of the workpiece after common lathe processing

Figure 5: The machined workpiece.

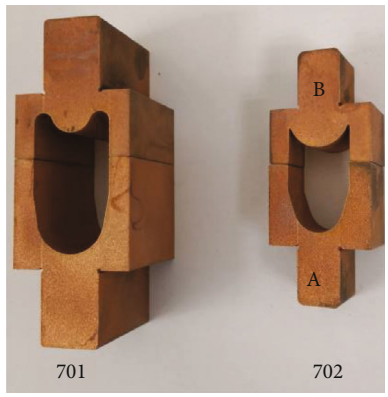

Figure 6: Copper electrodes used in EDM.

performed for the blade and the specimen. Additionally, the microstructural structures of the specimen are also analyzed with the SEM. Based on the finite element analysis, a more experimental test is performed on the specimen to verify the analyses' reasonability.

3. Preparing Blade Specimen

3.1. Designing the Blade Model. In real applications, the corner cracks are present at corner "*a*" as displayed in Figure 1. Thus, to reproduce this failure mode at the laboratory, the specimen is carefully designed based on the features of the blade. Detailed ideas behind the design are summarized as follows:

(1) The length of each part of the specimen

The length of the specimen is taken as 138 mm by reference to the material experiments and the machining conditions. Two ends of the specimen are the clamping parts, whose length is set to 53 mm because at this length, the specimen can be readily grasped by the test machine. The tested segment is the same with the real turbine blade. The remaining are the transition parts.

(2) The other design considerations

The two clamping segments are coaxial, and the center of gravity of the tested part lies on the coaxial line to ensure the exerted loads can model a reasonable centrifugal force; the chamfers of the tested part at the leading and trailing edge are designed to be 0.2 mm.

Detailed features of the blade specimen are displayed in Figure 3.

3.2. Designing the Machining Tools. To machine the blade specimen, a couple of copper tungsten electrode 702 made of T1 are designed according to the profile of the blade airfoil. The layouts of the electrode are displayed in Figure 4.

As displayed in Figure 4, the suction and the pressure side of the specimen are separately machined with the tools in (a) and (b). The design requirement is that the two sides finally form the needed airfoil. Note that the surface roughness of electrode 702 is *Ra* 0.3.

To make the load transition smooth, the other copper tungsten electrode 701 made of T1 is designed, which has a similar profile to 702. The machining requirements for 701 are not strict, so its layouts are not displayed.

3.3. Machining Equipment. The EDM process was implemented with the Electrical Discharge Machine GW735 which is developed by the BMTI PRECISION MECHATRNICS CO.LTD. The performances of GW735 are listed in Table 1.

3.4. Machining Blade Specimen. To improve the machining efficiency, the 304SS round bar was first machined by using the common lathe to obtain the specimen clamping parts. The machining parameters are displayed in Figure 5(a). The appearance of the workpiece after the common lathe machining is shown in Figure 5(b).

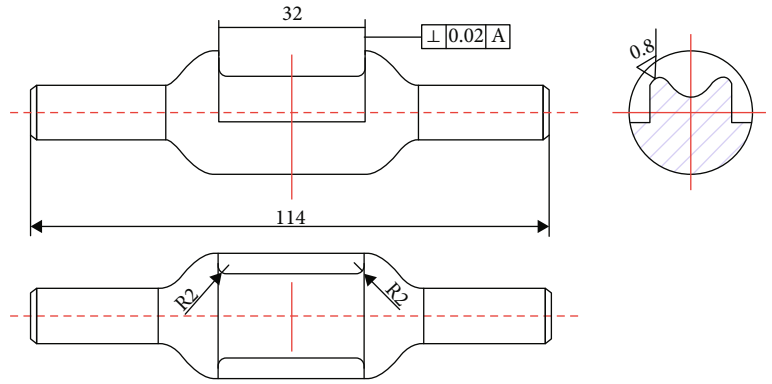

Figure 7: Using electrodes 701 to machine the transition segments in immersion oil.

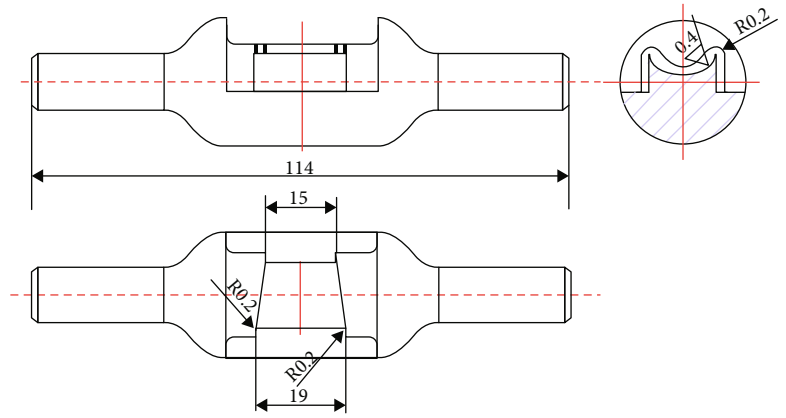

Figure 8: Using 702 to machine the pressure side in immersion oil.

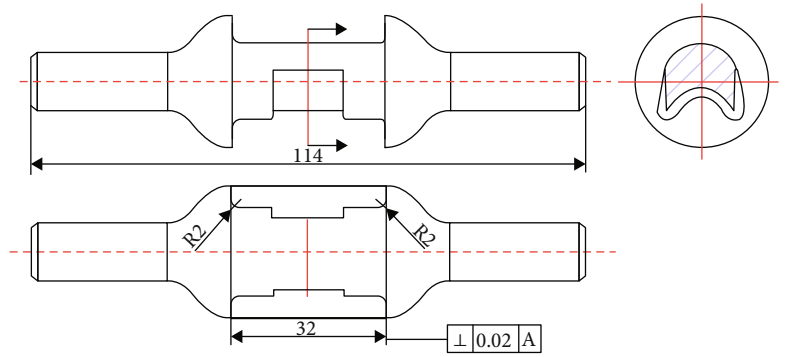

Figure 9: Using to machine the transition segments in immersion oil.

Then, the workpiece was machined by using the EDM process. In the EDM process, two couples of copper tungsten electrodes (Figure 6) are machined based on the layouts of electrode Figure 4. These electrodes are all machined by using the Wire cut Electrical Discharge Machine. During the process for 702, each effective electrode surface (i.e., the surfaces used to machine the tested parts) was machined by a three-step wire cutting from rough to fine to achieve the surface roughness *Ra* 0.3.

In the EDM process, the machining parameters should be carefully controlled to ensure the design requirements. Indeed, the discharge intensity, the pulse duration, the peak current, etc., significantly influence the processing quality. Generally, the relation of the roughness and the machining parameters reads,

$$R_{\max} = K_R t^{0.3} i^{0.4}, \tag{1}$$

where $R_{\max}$ is the peak-to-valley roughness, K_R is a constant 2.3, t is the pulse on time (μs), and i is the peak current (A). The relation between R_a and $R_{\max}$ is expressed as,

$$R_a = \frac{R_{\max}}{6 \sim 8}. \tag{2}$$

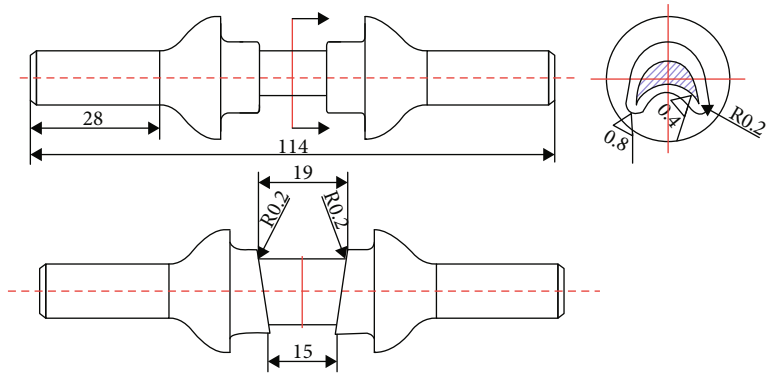

Figure 10: Using 702 to machine the suction side in immersion oil.

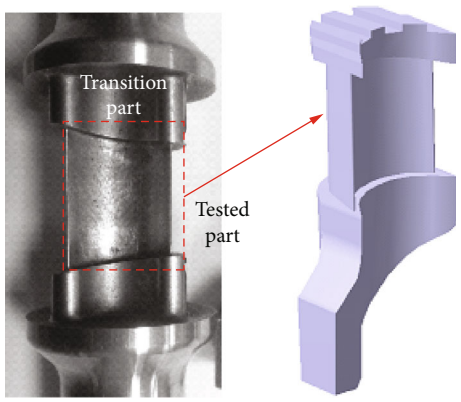

Figure 11: Blade model and the specimen.

Different from the previous literature, the aim of the work attempts to find a feasible method to machine the specimen for an impulse turbine blade. Therefore, the machining parameters are determined based on the authors' following experience:

(1) The initial discharge parameters are determined according to the requirements of maximum current density and machining efficiency that the electrode can bear

(2) The final discharge parameters are determined according to the blade surface quality requirements (roughness)

(3) The number of electrodes is determined according to the difference of surface roughness corresponding to the initial and final parameters (the larger the difference is, the more electrodes are used)

(4) Between the initial parameters and the final parameters, some transition parameters are selected, and the machining depth is determined according to the discharge gap

After several trials, the major EDM process parameters are determined as follows: (1) peak current: 1 A; (2) pulse on time: 0.8 μs; (3) pulse off time: 1.6 μs; (4) capacitance value: 1 nF. Also, other relevant parameters are as follows: (1) material removal rate: 0.3 mm^{-3}/min; (2) tool wear rate: 35%; (3) surface roughness: *Ra* 0.4. Although the surface roughness has agreed well with Eqs. (1) and (2), the sandblasting treatment is employed to release the residual stresses and remove the defects from the specimen. The parameters of the sandblasting process are as follows: (1) abrasive: 60-80 mesh brown corundum; (2) process pressure: 0.4-0.7 MPa; (3) angle between nozzle and workpiece: 30-45 degrees; (4) distance between nozzle and workpiece: 15 cm; (5) air consumption: 1.5 m^3/min.

The machining programme mainly consists of five steps.

Step 1. Machining side "P" of the transition segment.

The transition connects the clamping part and the tested blade model, which makes the loads transfer from the test machine to the specimen more smoothly. The side "*P*" was first machined as displayed in Figure 7. Note that "*P*" denotes the transition part lies on the side of the pressure side of the specimen.

Step 2. Machining the specimen pressure side.

After machining the transition part "*P*," then the pressure side of the tested part was machined. The process is schematically displayed in Figure 8.

Step 3. Machining side "S" of the transition segment.

Similar to step 1, the side "*S*" was machined as displayed in Figure 9. Note that "*S*" denotes the transition part lie on the side of the suction side of the specimen.

Step 4. Machining the suction side.

After machining the transition part "*S*," then the suction side of the tested part was machined. The process is schematically displayed in Figure 10.

Step 5. The sandblasting treatment.

After the EDM process, the sandblasting treatment is employed to release the residual stresses and remove the defects from the specimen, which improves the fatigue resistance.

4. Results and Discussion

4.1. Geometrical Feature Analysis. After the EDM process, the tested part of the blade specimen is illustrated in Figure 11(a). As a comparison, the 3D blade model is displayed in Figure 11(b) as well.

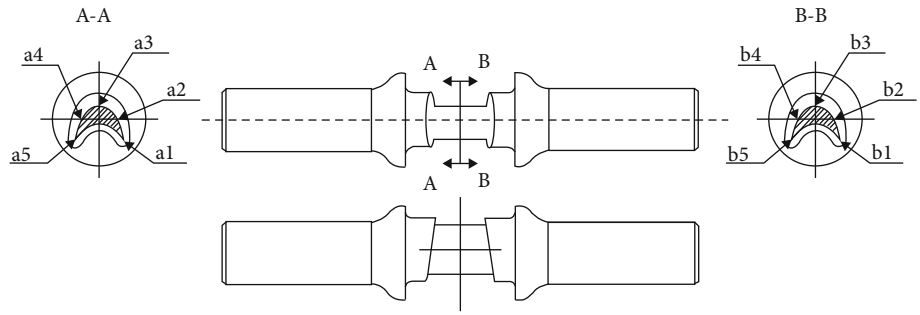

Figure 12: Positions to be measured.

Table 2: Radii of the chamfers.

Position	a1	a2	a3	a4	a5	b1	b2	b3	b4	b5
Value/mm	0.26	0.65	0.73	0.67	0.26	0.26	0.59	0.64	0.68	0.20

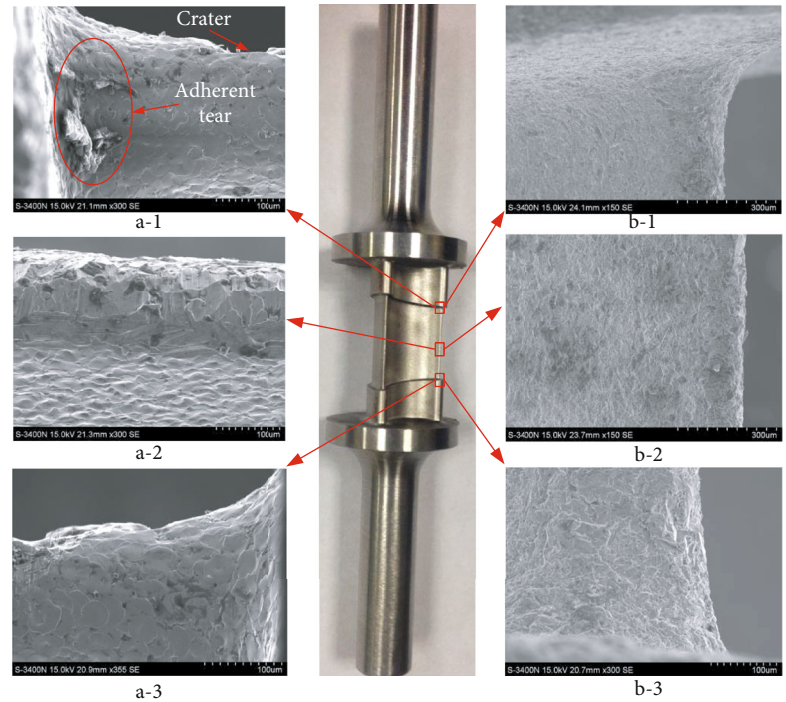

(a) Microstructures after the EDM process

(b) Microstructures after sandblasting treatment

Figure 13: Microstructures on the surface of the blade specimen. (a) Microstructures after the EDM process. (b) Microstructures after sandblasting treatment.

From the viewpoint of geometry, it is seen from Figure 11 that the tested section is consistent with the real blade airfoil. By comparing Figure 2 with Figure 3, it is seen that the EDM process obtains the fundamental geometrical details.

Generally, the blade specimen is used to test the aerodynamical, mechanical, and working life-related properties of the blade. The size of the chamfer between the tested and transition part has a significant effect on these properties because it determines the level of the stress concentration. Thus, ten positions are selected to measure the radii of the chamfer (Figure 12). Note that the designed value of chamfer is 0.2 mm.

Table 2 gives the radii of the chamfer, which are measured with the optical magnifier.

From Table 2, it is seen that the radii of the chamfers at the leading and trailing edge are close to the designed value, whereas they are larger than 0.2 mm at the other measure points. To study the influence of these radii on the fatigue-related problem, some finite element analyses and experimental tests are performed on the specimen.

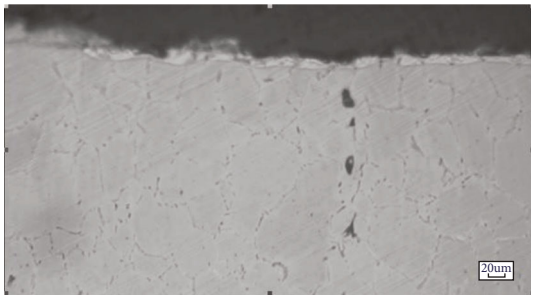

Figure 14: Microphotograph of the recast layer after EDM [23].

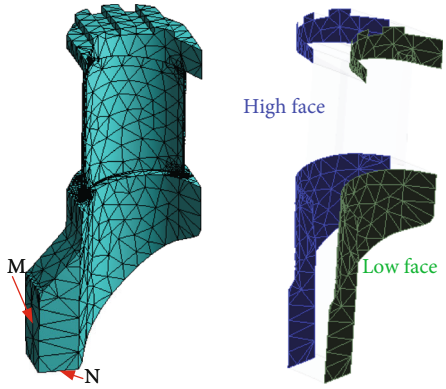

Figure 15: Grids of the turbine blade model and cyclic symmetric mesh for analysis.

4.2. Benefit and Cost Analysis

4.2.1. Benefit. This method significantly reduces the experimental time consumption for the turbine blade. The specimen can be prepared within 5 days: cutting electrode—3 days; manufacturing—2 days. Additionally, the fatigue test can be carried out within 2 days. However, dozens of days will be needed if we apply the integrated turbine to test the fatigue life of the blade. Thus, this method in the current work reduces the experimental time consumption.

4.2.2. Cost. This method significantly reduces the fatigue test cost, because it performs the test on the individual blade but not the integrated turbine. To the best knowledge of the authors, the manufacture cost of the similar rocket turbine is around hundreds of thousands of RMB. However, the cost of the specimen is only 2500 RMB. Because the turbine consists of 91 blades, to obtain the same number of fatigue experimental results, the cost of the experiment on the real turbine is roughly 16562 ($91 \times 91 \times 2$) times as much as the specimen.

4.3. Microstructure Analysis. The microstructures are detected with SEM to find out the change of the surfacial microstructures before and after the sandblasting treatment. The SEM results are separately displayed in Figures 13(a) and 13(b).

From Figures 13(a) and 13(b), it can be found that the microstructures become more homogeneous after the sandblasting treatment. In Figure 13(a), there exists an adhesion tear at the corner of the leading edge. Additionally, some craters randomly spread on the airfoil. From [22], it is seen that in the real turbine, the highest temperature is present at the leading edge of the blade is the highest. In the start-up and shutdown stage, the temperature gradient of the leading and trailing edge is relatively large, which leads to high thermal stress. Therefore, the leading and trailing edges are more vulnerable. For the specimen, the sizes of these irregular defects are only several tens of micrometers. According to the fatigue theory, these defects have some harmful effects on high cycle fatigue (HCF) while little on low cycle fatigue (LCF) because the former is much more sensitive to the surface quality.

Table 3: Chaboche elasto-plastic model parameters.

Hardning parameter	Value	Rate parameter	Value
C^1	165362	γ^1	7937
C^2	60140	γ^2	280
C^3	4322	γ^3	2.5

In [23], it is found that the surface of the sample machined by the EDM process actually consists of three layers. The outmost layer is the recast layer, and then, the medium is the quenching layer, and the deeper regime is the annealed layer. The schematic microphotograph of the surface layer is simply displayed in Figure 14.

The recast layer can significantly increase the hardness and the roughness of the surface, and the depth of the top recast layer is greatly influenced by the pulse energy and duration. Moreover, the working discharge power has a close relationship with the depth of the three layers, which influences the fatigue properties.

To the best knowledge of the authors, numerous tests and detections should be performed by spending much time and huge cost if one wants to figure out how the microstructure influences the fatigue. However, it is not the concerned problem for the current work. Thus, this issue is not considered herein. The reasons for using the sandblasting treatment are that in [24], the authors suggest the following: (1) the fields of tensile residual stresses are responsible for the stress corrosion cracking and (2) the metallurgical transformation on the surface significantly reduces the endurance limit of the component machined with the EDM process. After the sandblasting treatment, the residual stresses are released and the defects are removed from the surface, which improves the fatigue resistance to some extent.

4.4. Finite Element Analysis

4.4.1. Finite Element Analysis for Turbine Blade. To provide a reference for the experimental test, the working characteristics of the blade are numerically studied. To reduce the computational time, just one turbine blade is used in the simulation. In order to ensure the same mechanical properties occur at high face "H" and low face "L," the "cyclic symmetric structural analysis" is employed.

The blade model is meshed with the 3D 10-node tetrahedral element, and 16557 elements are obtained in total. The mesh for use is displayed in Figure 15.

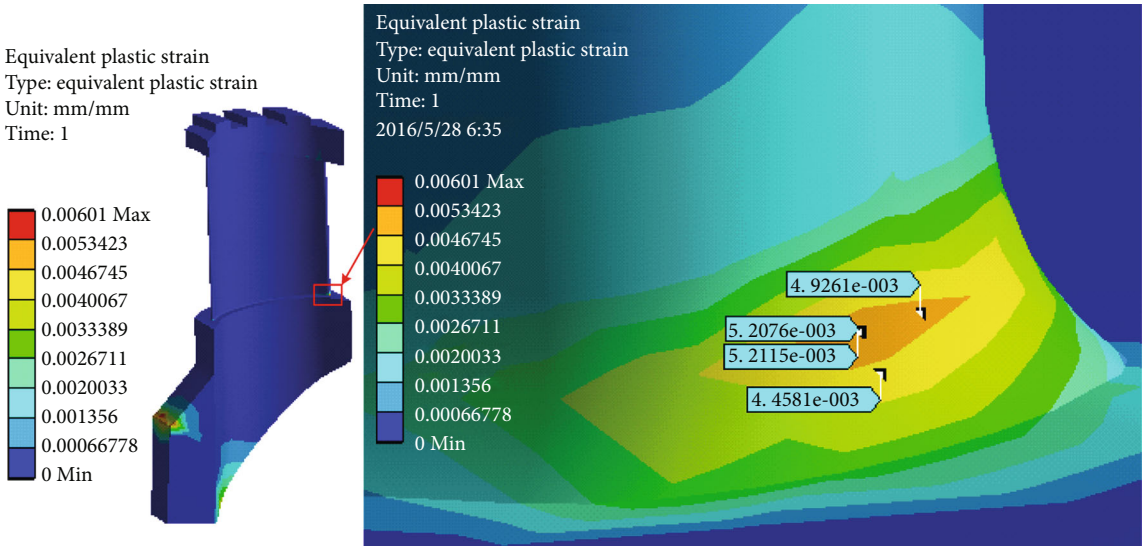

Figure 16: Equivalent plastic strains on the blade surface.

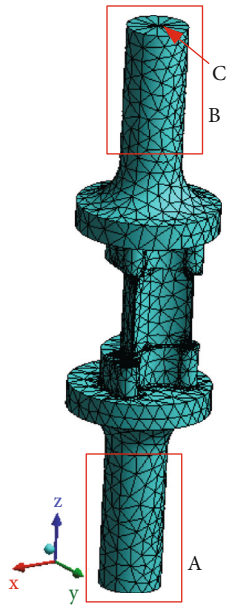

Figure 17: Grids of the blade specimen.

As displayed in Figure 15, to obtain a larger grid density, the chamfers are selected to be remeshed. To complete the "cyclic symmetric analysis," the ANSYS Parameters Design Language (APDL) command "CPCYC" is used to establish a coupled degree-of-freedom (DOF) for the two faces. The associated command streamlines are given as follows:

allsel, all
cmsel, s, lowface
cmsel, a, highface
cpcyc, all, 0.05, 12,, 4,, 0

From the command streamlines, it is seen that the coincidence tolerance is set to 0.05. The node location increment is set to a 4-degree angle which agrees to 90 blades. The blade speed is 19800 rpm.

The Chaboche kinematic hardening model parameters for 304SS are adopted from [25], which are displayed in Table 3.

Additionally, the isotropic hardening model parameters Q and b are, respectively, set to 75 MPa and 44. Detailed explanations of the Chaboche combined hardening model can be found from [25].

Faces "M" and "N" are set to be fixed support in the simulation, because they have little effect on the critical portions. Figure 16 displays the equivalent plastic strain nephogram of the blade.

From Figure 16, it is obvious that the maximum equivalent plastic strain is around 5.21×10^{-3} mm/mm, which is present at the chamfer close to the hub. As stated in [26], the plastic strain represents the irreversible damage caused by dislocation movement, which is critical to determine the working life of the blade. Thus, having the same total strain at the critical position is the basic principle to perform the fatigue experimental test. Different from [27], to ensure the centrifugal strains at the root of the leading edge of the blade and the specimen are the same, the experimental loading exerted on the specimen is determined by the following simulation method.

4.4.2. Finite Element Analysis for Specimen. There are two purposes to carry out the FEA for the specimen: (1) verifying whether the same maximum plastic strain is present at the corner of the leading edge and (2) obtaining the loads employed in the fatigue test.

Prior to the simulation, the blade specimen is first meshed with the 3D 10-node tetrahedral element, and 33970 elements are obtained in total (Figure 17).

In the simulation, part "A" from Figure 17 is fixed and "B" has the displacement freedom along the z direction only. The load exerted on the end face "C" is determined by using the trial-and-error method. The final load for use is 13407 N, which ensures the maximum plastic strain is present at the

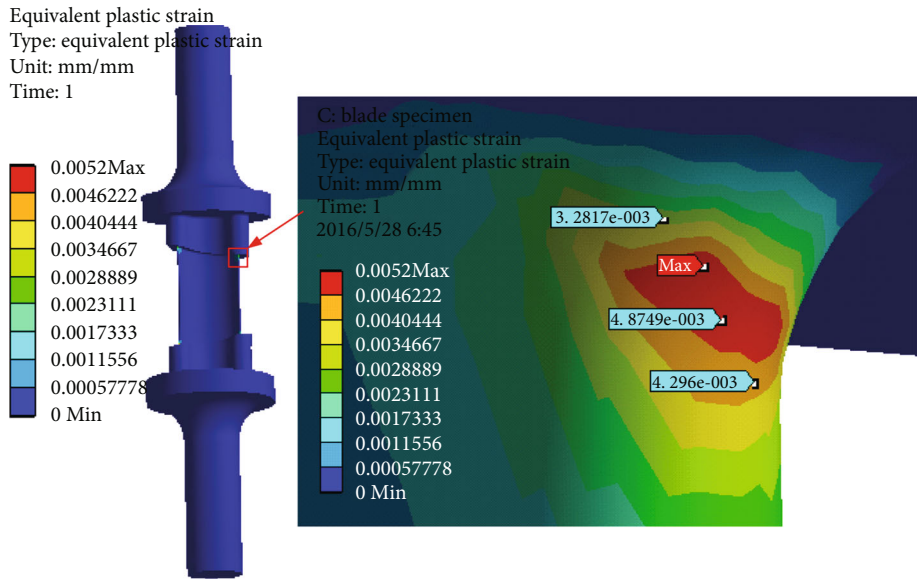

Figure 18: Equivalent plastic strains of the specimen.

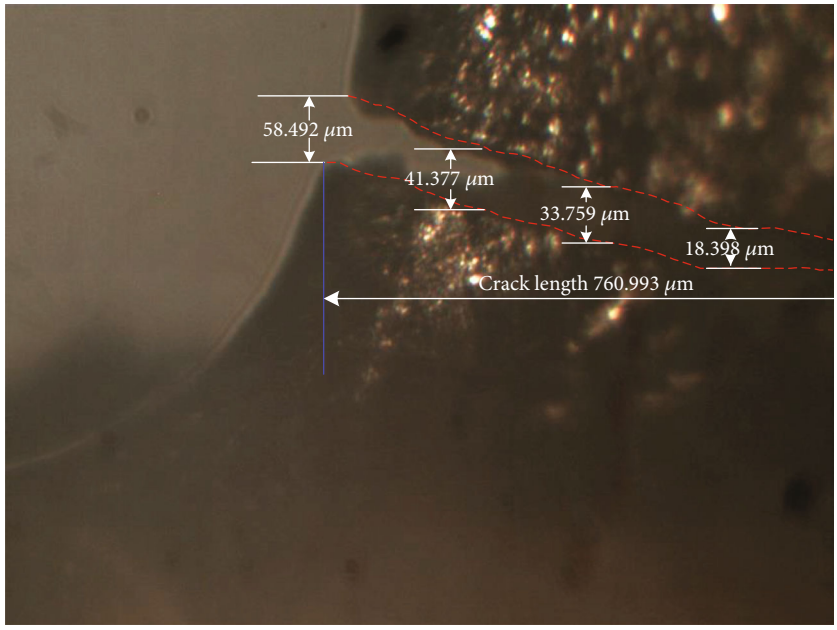

Figure 19: The corner crack at the leading edge of the specimen in the fatigue test.

same position with the blade. Figure 18 shows the equivalent plastic strain nephogram of the specimen.

From Figure 18, it is seen the maximum equivalent plastic strain is around 5.2×10^{-3} mm/mm, which occurs at the corner of the leading edge and nearly equals to that on the blade (Figure 16). From the fatigue theory, the minimum fatigue life should be present at the position having the maximum plastic strain.

4.5. Experimental Test. In 2020, Salehnasab and Poursaeidi [28] pointed out that the high centrifugal stress and thermal loads in start-up and shutdown are responsible for the low cycle life of blades. Thus, in the current work, the fatigue verification test at room temperature is conducted. Based on Section 4.4, the experimental fatigue test is performed under the following conditions: 13407 N load amplitude, 0.25 Hz frequency, and 0 load ratio. At the 10113th cycle, a corner crack length of 760.993 μm occurred at the position of the maximum equivalent plastic strain. The optical observation of the crack is displayed in Figure 19.

From the above analyses, it is seen the validity of using the EDM process to machine the blade specimen is supported by (1) the geometry of the tested blade model is consistent with the real turbine blade and (2) both the blade and the specimen have the same simulated critical portion, and the fatigue crack occurs at this position. Indeed, in the real

application, the turbine blade is also polished with the sandblasting method.

From [29], it is seen that the crack sizes during the crack propagation obtained from the fatigue test are important for the durability and damage tolerance, which determine the crack growth control curve. Through numerous tests, the properties of the fatigue and the fracture will be familiar to the engineers. As stated in [30], the variable amplitude fatigue crack growth rate and the methods of starting crack sizes in damage tolerance and durability analysis are analyzed. The authors conducted a variable stress-controlled fatigue test on the specimen made from 7050-T7451 aluminum alloy. By fitting the crack growth rate $(\mathrm{d}a/\mathrm{d}t)_i$, the authors obtained the constants of the EIFS (Equivalent Initial Flaw Size) distribution. Thus, the current work is important to reveal the crack propagating history of the impulse turbine blade, which provides a valuable reference for designing a long-time service blade.

5. Conclusions

The reusability of the turbine blade of the rocket engine is rarely investigated at the laboratory. Thus, in the current work, a specimen was designed and machined for a small impulse turbine blade for reuse. After carefully comparing different processing methods, the electrical discharge machining (EDM) is selected to machine the blade specimen. To machine the specimen, two couples of electrodes were developed using the wire cutting processing. Based on the machining programme, the blade specimen was obtained. And then the sandblasting treatment was employed to release the residual stresses and remove the defects on the surface. In order to verify the feasibility of the specimen for the fatigue test, a finite element analysis method was used to separately analyze the stress-strain response of the blade and the specimen, which help to find out the experimental conditions in the fatigue test. Finally, the microstructures of the specimen are detected with the SEM. Based on this investigation, the following three conclusions are drawn:

(1) The specimen of this type of small impulse turbine blade is unable to be machined with the welding method because it destroys the details and the mechanical properties of the specimen

(2) The maximum plastic strain is present at the leading edge close to the hub, which is susceptible to be damaged. These facts also supported by the fatigue test, where a corner crack length of 760 μm occurs at the 10113th cycle

(3) The finite element analysis and the experimental test directly reflect the feasibility of using the EDM process method to machine specimen for the small impulse turbine blade

The proposed method provides a reference to assess the reusability of an impulse turbine blade in aerospace. It can also be extended to other industries, such as the torpedo turbine and nuclear-power generation.

Data Availability

All data are provided by the authors.

Conflicts of Interest

The authors declare that they have no conflicts of interest.

Acknowledgments

The authors express their sincere gratitude to Ms. Bai in The National Center for Nanoscience and Technology of China for the help of SEM application instruction.

References

[1] C. Cao and X. J. Yan, *Creep/Fatigue Tests on Full Scale Hollow Turbine Blades Considering Temperature Gradient, ASME Turbo Expo 2016*, Turbomachinery Technical Conference and Exposition, Seoul, South Korea, 2016.

[2] R. Q. Wang, F. L. Jing, and D. Y. Hu, "Experimental setup for testing thermo-mechanical fatigue of single crystal turbine blades," *Hangkong Dongli Xuebao/Journal of Aerospace Power.*, vol. 28, pp. 252–258, 2013.

[3] F. L. Jing, R. Q. Wang, and D. Y. Hu, "A thermo-mechanical fatigue life assessment method for single crystal turbine blades," *Journal of Aerospace Power*, vol. 31, pp. 299–306, 2016.

[4] S. Sanaye and S. Hosseini, "Prediction of blade life cycle for an industrial gas turbine at off-design conditions by applying thermodynamics, turbo-machinery and artificial neural network models," *Energy Reports*, vol. 6, pp. 1268–1285, 2020.

[5] H. M. Tawancy and L. M. Al-Hadhrami, "Comparative performance of turbine blades used in power generation: damage vs. microstructure and superalloy composition selected for the application," *Engineering Failure Analysis*, vol. 46, pp. 76–91, 2014.

[6] P. Y. Zhang, X. Zhou, X. D. Wang, Y. W. Lu, X. Cheng, and W. Q. Zhang, "Study on the microstructural degradation and rejuvenation heat treatment of directionally solidified turbine blades," *Journal of Alloys and Compounds*, vol. 829, article 154474, 2020.

[7] R. Q. Wang, K. H. Jiang, F. L. Jing, and D. Y. Hu, "Thermomechanical fatigue failure investigation on a single crystal nickel superalloy turbine blade," *Engineering Failure Analysis*, vol. 66, pp. 284–295, 2016.

[8] S. Kumar, R. Singh, T. P. Singh, and B. L. Sethi, "Surface modification by electrical discharge machining: a review," *Journal of Materials Processing Technology*, vol. 209, no. 8, pp. 3675–3687, 2009.

[9] N. M. Abbas, D. G. Solomon, and M. F. Bahari, "A review on current research trends in electrical discharge machining (EDM)," *International Journal of Machine Tools and Manufacture*, vol. 47, no. 7-8, pp. 1214–1228, 2007.

[10] M. Tanjilul, A. Ahmed, A. S. Kumar, and M. Rahman, "A study on EDM debris particle size and flushing mechanism for efficient debris removal in EDM-drilling of Inconel 718," *Journal of Materials Processing Technology*, vol. 255, pp. 263–274, 2018.

[11] N. Agarwal, M. K. Pradhan, and N. Shrivastava, "A new multi-response Jaya Algorithm for optimisation of EDM process

parameters," *Materials Today: Proceedings*, vol. 5, pp. 23759–23768, 2018.

[12] N. Nagaraju, S. Venkatesu, and N. G. Ujwala, "Optimization of process parameters of EDM process using fuzzy logic and Taguchi methods for improving material removal rate and surface finish," *Materials Today: Proceedings.*, vol. 5, pp. 7420–7428, 2018.

[13] M. Dastagiria, P. S. Raob, and P. M. Vallic, "Optimization of EDM process parameters by using heuristic approach," *Materials Today: Proceedings*, vol. 5, pp. 27036–27042, 2018.

[14] C. Prakash, S. Singh, M. Singh, V. Kartikey, G. Babulal, and S. Subhash, "Multi-objective particle swarm optimization of EDM parameters to deposit HA-coating on biodegradable Mg-alloy," *Vacuum*, vol. 158, pp. 180–190, 2018.

[15] M. Zhou, X. Mu, L. He, and Q. Ye, "Improving EDM performance by adapting gap servo-voltage to machining state," *Journal of Manufacturing Processes*, vol. 37, pp. 101–113, 2019.

[16] H. Gonzalea-Barrio, A. Calleja-Ochoa, A. Lamikiz, and L. N. Lopez-de-Lacalle, "Manufacturing processes of integral blade rotors for turbomachinery, processes and new approaches," *Applied Sciences*, vol. 10, pp. 1–21, 2020.

[17] X. J. Yan and J. X. Nie, "Creep-fatigue tests on full scale directionally solidified turbine blades," *Journal of Engineering for Gas Turbines and Power*, vol. 130, article 044501-1, 2008.

[18] E. S. Zink, D. Bourdon, V. N. Junior, D. F. Sias, W. Kitsche, and B. Wagner, "Study of manufacturing processes for liquid rocket turbopump impellers: test and analysis," *Journal of Aerospace Technology and Management*, vol. 12, pp. 1–12, 2020.

[19] H. Oguma, K. Tsukimoto, S. Goya, Y. Okajima, K. Ishizaka, and E. Ito, "Development of advanced materials and manufacturing technologies for high-efficiency gas turbines," *Mitsubishi Heavy Industries Technical Review*, vol. 52, pp. 5–16, 2015.

[20] M. G. Sharapov and V. M. Shvedikov, "The efficiency of gas jet shielding in argon-arc welding," *Welding International*, vol. 18, no. 8, pp. 635–640, 2004.

[21] K. Kalyani and G. S. Reddy, "Modelling and manufacturing of jet engine turbine blade using additive manufacturing," *International Journal of Innovative Science and Research Technology*, vol. 2, pp. 175–179, 2017.

[22] H. R. Alejandro, M. C. Zdzislaw, M. Rodolfo, and B. Eder, "Start-up and shut-down simulation of a thermal barrier coating gas turbine bucket using CFD code," in *Proceedings of the ASME 2008 Power Conference. ASME 2008 Power Conference*, pp. 75–83, Lake Buena Vista, Florida, USA, July 2008.

[23] J. Xia, *Research on Surface Quality of Superalloy GH4169 Machined by ECM&EDM, College of Mechanical and Electronic Engineering*, Nanjing University of Aeronautics and Astronautics, 2007.

[24] H. Sidhom, F. Ghanem, T. Amadou, and C. G. GBraham, "Effect of electro discharge machining (EDM) on the AISI316L SS white layer microstructure and corrosion resistance," *International Journal of Advanced Manufacturing Technology*, vol. 65, no. 1-4, pp. 141–153, 2013.

[25] S. J. Liu, G. Z. Liang, and Y. C. Yang, "A strategy to fast determine Chaboche elasto-plastic model parameters by considering ratcheting," *International Journal of Pressure Vessels and Piping*, vol. 172, pp. 251–260, 2019.

[26] J. Genée, L. Signor, and P. Villechaise, "Slip transfer across grain/twin boundaries in polycrystalline Ni-based superalloys," *Materials Science and Engineering: A*, vol. 701, pp. 24–33, 2017.

[27] W. Rongqiao, J. Fulei, and H. Dianyin, "In-phase thermal-mechanical fatigue investigation on hollow single crystal turbine blades," *Chinese Journal of Aeronautics*, vol. 26, pp. 1409–1414, 2013.

[28] B. Salehnasab and E. Poursaeidi, "Mechanism and modeling of fatigue crack initiation and propagation in the directionally solidified CM186 LC blade of a gas turbine engine," *Engineering Fracture Mechanics*, vol. 225, article 106842, 2019.

[29] A. Abdul-Aziz, *Structural Evaluation of a Space Shuttle Main Engine (SSME) High Pressure Fuel Turbopump Turbine Blade, NAS3-27186*, NYMA, Inc., Brook Park, OH, USA, 1996.

[30] J. P. Gallagher and L. Molent, "The equivalence of EPS and EIFS based on the same crack growth life data," *International Journal of Fatigue*, vol. 80, pp. 162–170, 2015.